On the Linkages between the Tropospheric Isentropic Slope and Eddy Fluxes of Heat during Northern Hemisphere Winter

DAVID W. J. THOMPSON AND THOMAS BIRNER

Department of Atmospheric Science, Colorado State University, Fort Collins, Colorado

(Manuscript received 13 July 2011, in final form 12 December 2011)

ABSTRACT

Previous studies have demonstrated the key role of baroclinicity and thus the isentropic slope in determining the climatological-mean distribution of the tropospheric eddy fluxes of heat. Here the authors examine the role of variability in the isentropic slope in driving variations in the tropospheric eddy fluxes of heat about their long-term mean during Northern Hemisphere winter.

On month-to-month time scales, the lower-tropospheric isentropic slope and eddy fluxes of heat are not significantly correlated when all eddies are included in the analysis. But the isentropic slope and heat fluxes are closely linked when the data are filtered to isolate the fluxes due to synoptic (<10 days) and low-frequency (>10 days) time scale waves. Anomalously steep isentropic slopes are characterized by anomalously poleward heat fluxes by synoptic eddies but anomalously equatorward heat fluxes by low-frequency eddies. Lag regressions based on daily data reveal that 1) variations in the isentropic slope precede by several days variations in the heat fluxes by synoptic eddies and 2) variations in the heat fluxes due to both synoptic and low-frequency eddies precede by several days similarly signed variations in the momentum flux at the tropopause level.

The results suggest that seemingly modest changes in the tropospheric isentropic slope drive significant changes in the synoptic eddy heat fluxes and thus in the generation of baroclinic wave activity in the lower troposphere. The linkages have implications for understanding the extratropical tropospheric eddy response to a range of processes, including anthropogenic climate change, stratospheric variability, and extratropical sea surface temperature anomalies.

1. Context

Feedbacks between the mean flow and the wave fluxes of heat and momentum play a fundamental role in the general circulation of the extratropical troposphere (e.g., Holton 2004, ch. 10; Vallis 2006, ch. 12). For example, wave activity is predominantly generated near the surface in regions of large isentropic slopes (Fig. 1a; e.g., Stone 1978). Much of the wave activity generated in the lower troposphere propagates vertically and is thus associated with poleward fluxes of heat in the free troposphere. If the wave activity dissipates in the upper troposphere at roughly the same latitude range as the wave source (Fig. 1b), then the westward torque aloft drives a residual (mass) circulation with rising motion equatorward of the wave source and sinking motion poleward of the wave source. The anomalous vertical motion acts to reduce the lower-tropospheric isentropic slope that generated the wave activity in the first place. As such, the residual circulation induced by the wave breaking aloft acts as a negative feedback that attenuates lower tropospheric baroclinicity.

A somewhat different relationship holds between the lower-tropospheric isentropic slope and the wave fluxes of momentum. For example, assume that a component of the upper-tropospheric wave activity in Fig. 1b propagates equatorward near the tropopause. The equatorward wave propagation is associated with poleward momentum fluxes that converge at the source latitude (Fig. 1c). Viewed in isolation, the momentum fluxes induce a residual circulation that acts to reinforce rather than damp the lower-tropospheric isentropic slope in the wave source region (Fig. 1c). Hence, the residual circulation induced by the momentum flux convergence aloft acts as a positive feedback that increases lower-tropospheric baroclinicity.

In the climatological mean, the wave driving due to the vertical convergence of the wave flux (i.e., the vertical convergence of the heat flux) is larger than that due

Corresponding author address: David W. J. Thompson, Colorado State University, Department of Atmospheric Science, Campus Delivery 1371, Fort Collins, CO 80523.
E-mail: davet@atmos.colostate.edu

DOI: 10.1175/JAS-D-11-0187.1

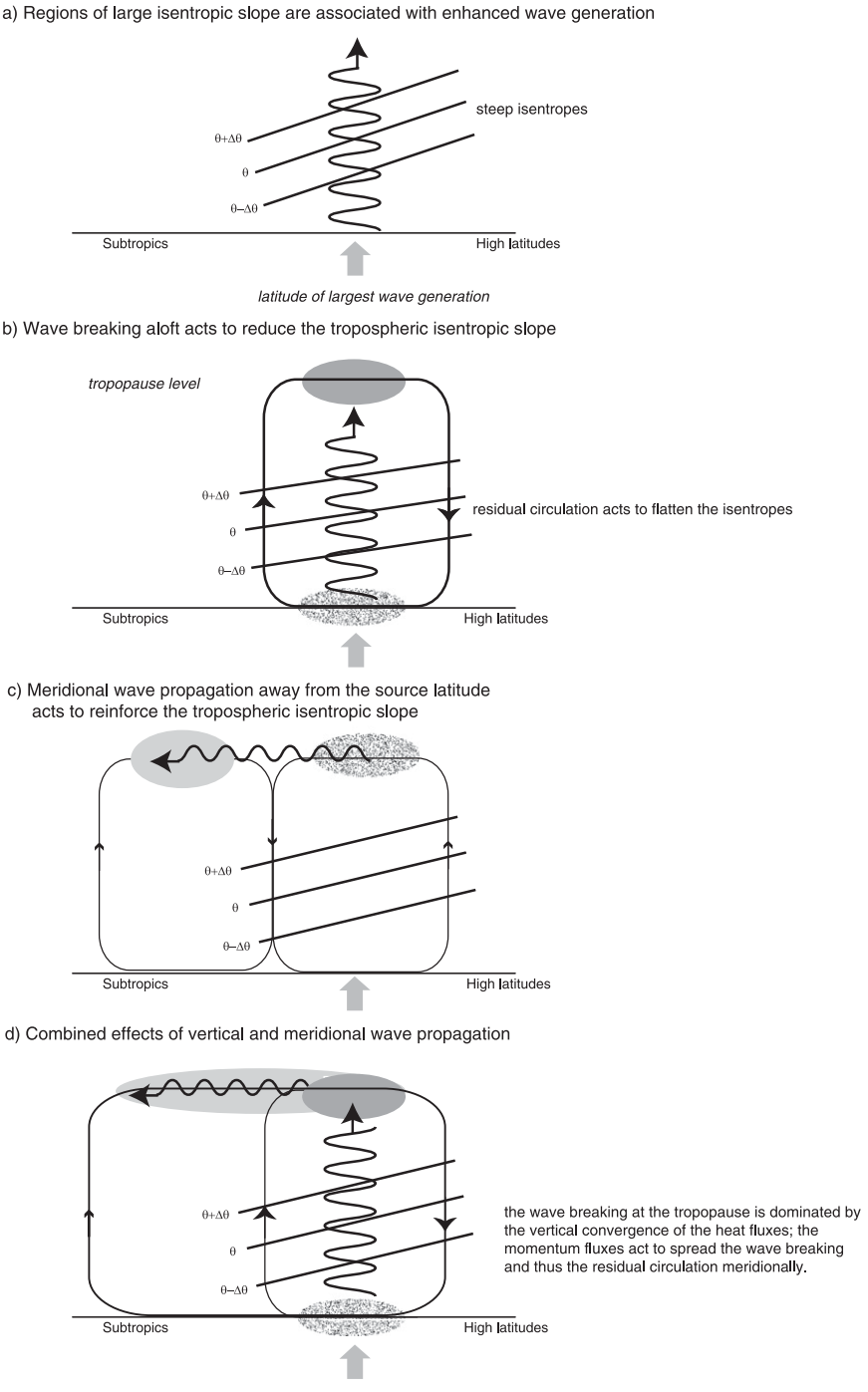

FIG. 1. Schematics of the interactions between the isentropic slope and the wave fluxes of heat and momentum. Schematics denote distinct dynamical situations and do not necessarily reflect a series of events. Sloping lines indicate isentropic surfaces, wavy lines indicate the direction of the wave fluxes, shading (stippling) denotes regions of Eliassen–Palm (EP) flux convergence (divergence), and rounded rectangles indicate the residual circulation. See text for details.

to the meridional divergence of the wave flux (i.e., the meridional convergence of the momentum flux) (e.g., Edmon et al. 1980). Hence, the total wave driving is westward at the tropopause level, but the momentum fluxes spread the wave driving over a wider range of latitudes than the wave source (Fig. 1d). Since the momentum fluxes spread the wave driving meridionally, it follows that they also reduce the amplitude of the

compensating poleward mass flux at the latitude of the wave source. As a result, the wave-driven residual circulation attenuates the lower-tropospheric isentropic slope, but not as much as it would if all the wave-breaking was concentrated at the latitude of the wave source (e.g., Robinson 2000, 2006).

The relationships among the isentropic slope, tropospheric wave generation, and tropospheric wave dissipation reviewed schematically in Fig. 1 are known to play a key role in determining the climatological-mean extratropical circulation. The largest eddy fluxes of heat are roughly collocated with the regions of largest lower-tropospheric baroclinicity (Kushner and Held 1998); the largest momentum fluxes are closely collocated with the extratropical storm tracks (e.g., Lau et al. 1978; Lim and Wallace 1991). However, the role of the isentropic slope in driving variability in the extratropical wave fluxes of heat and momentum remains unclear. The amplitude of such a feedback is important, since the sensitivity of the eddies to variations in the isentropic slope is theorized to play a potentially key role in driving the following: 1) the internal feedbacks that give rise to the annular modes (e.g., Robinson 2000, 2006; Lorenz and Hartmann 2001, 2003); 2) the storm track response to extratropical sea surface temperature anomalies (e.g., Kushnir et al. 2002, and references therein; Brawshay et al. 2008); 3) the extratropical tropospheric response to stratospheric variability (e.g., Song and Robinson 2004); and 4) the storm track response to increasing greenhouse gases (e.g., Kushner et al. 2001; Yin 2005; Frierson 2006; Lu et al. 2008, 2010; Chen et al. 2010; O'Gorman 2010; Scaife et al. 2012; Butler et al. 2011).

The primary purpose of this study is to quantify the observed relationships between variability in the isentropic slope and the eddy fluxes of heat and momentum in the Northern Hemisphere (NH) tropospheric circulation. The results imply that low-frequency time scale eddies primarily force anomalies in the baroclinicity, whereas synoptic time scale eddies respond to anomalies in the baroclinicity. The dataset is discussed in section 2; results are presented in section 3; implications of the results for climate variability are discussed in section 4.

2. Data and analysis

The primary dataset is 4-times-daily values of the interim European Centre for Medium-Range Weather Forecasts (ECMWF) Re-Analysis (ERA-Interim) data from 1 January 1989 to 31 December 2009 (see *ECMWF Newsletter,* No. 110; Dee et al. 2011). The reanalyses products are available on a 1.5° × 1.5° mesh, and are daily and zonally averaged before computing regressions and correlations. The zonal mean fluxes of heat and momentum are defined as $[v^*T^*]$ and $[u^*v^*]$, respectively, where brackets denote the zonal mean and stars denote the departure from the zonal mean. The fluxes are calculated at 4-times-daily resolution before being daily averaged. Anomalies are defined throughout the study as departures from the long-term mean seasonal cycle. All results are calculated for the Northern Hemisphere, for anomalies, and for the winter months of December–February (DJF).

The wave fluxes of heat due to synoptic and low-frequency time scale eddies were estimated by decomposing the fluxes as follows:

$$[v^*T^*] = [v_s^*T_s^*] + [v_l^*T_l^*] + \text{cross terms},$$

where the synoptic time scale (denoted by subscript s) is defined as less than 10 days and the low-frequency time scale (denoted by subscript l) is defined as longer than 10 days. The time filtering was done using an eighth-order Butterworth filter with a cutoff frequency of 10 days. A similar procedure was applied to the eddy fluxes of momentum.

Note that the synoptic eddies exhibit variability on time scales longer than 10 days, even though the wind and temperature time series have both been 10-day high-pass filtered. As noted in Lorenz and Hartmann (2001), the redness of the synoptic eddy fluxes is consistent with a positive feedback between the synoptic eddy fluxes and the mean flow. The cross terms are generally small and are not considered here.

We exploit the ERA-Interim products in both isentropic and pressure coordinates. To orient the reader to our use of both coordinate systems, Fig. 2 shows the DJF-mean, zonal-mean Northern Hemisphere circulation as a function of (left) latitude and pressure and (right) latitude and potential temperature. In both panels, the height of the tropopause (thick line) is approximated as the level where potential vorticity is equal to 2 potential vorticity units (PVU; 1 PVU = 10^{-6} K kg^{-1} m^2 s^{-1}). Key surfaces used in the results section include 1) the 285-K isentrope, which extends from the surface in the subtropics near 35°, spans the lower troposphere at mid- to high latitudes, and reaches the 500-hPa level at polar latitudes; 2) the 700-hPa level, which lies near the top of the atmospheric boundary layer; and 3) the 300-hPa level, which lies in the upper-troposphere/lower-stratosphere region.

Variability in the strength of the extratropical stratospheric vortex is defined as the leading principal component time series of the zonal-mean 10-hPa geopotential height field. The index is generated according to Baldwin and Thompson (2009) and is referred to as the northern annular mode index at 10 hPa (NAM10). By definition,

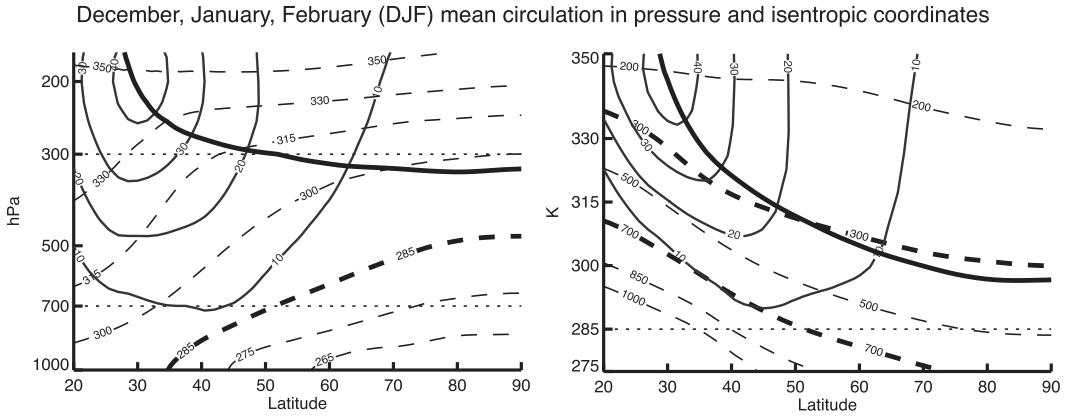

FIG. 2. NH DJF-mean, zonal-mean circulation in (left) pressure and (right) isentropic coordinates. Dashed lines indicate (left) isentropic surfaces and (right) pressure surfaces, thin solid lines indicate the zonal wind, and the thick solid lines indicate the 2-PVU isoline and thus approximate the height of the dynamical tropopause. The isentropic levels in the right panel correspond to the isentropic levels available in the ERA-Interim dataset.

positive values of the NAM10 index denote a stronger than normal stratospheric vortex, and vice versa. [Note that the results in Fig. 9 are based on inverted values of the NAM10 index (i.e., the index is multiplied by −1) so that the regression coefficients correspond to weakenings of the stratospheric circumpolar zonal flow.]

Statistical significance of key results is assessed using a one-tailed test of the *t* statistic. The effective degrees of freedom are estimated using the autocorrelation characteristics of the respective time series. By definition, standardized time series have a mean of zero and standard deviation of one.

3. Observed linkages between variability in the tropospheric isentropic slope and eddy fluxes of heat and momentum

The meridional slope of extratropical isentropic surfaces provides a succinct measure of the tendency of the atmosphere to generate wave activity (e.g., Stone 1978; Stone and Nemet 1996). The isentropic slope is—by definition—given as (minus) the ratio of the meridional and vertical gradients in potential temperature. Increases in the amplitude of the meridional potential temperature gradient (i.e., the baroclinicity) and decreases in the vertical potential temperature gradient (i.e., the static stability) both increase the isentropic slope and thus the instability of the flow to the generation of baroclinic waves. The meridional slope of the isentropes is related to the available potential energy of the general circulation (e.g., Lorenz 1955) and is closely related to the Eady growth rate (the Eady growth rate is proportional to the meridional temperature gradient divided by the buoyancy frequency; Lindzen and Farrell 1980).

The isentropic slope is calculated here as the meridional gradient in pressure along isentropic surfaces; that is,

$$-\frac{(\partial\theta/\partial y)_p}{(\partial\theta/\partial p)_y} = \left(\frac{\partial p}{\partial y}\right)_\theta \equiv s_p,$$

where θ denotes potential temperature, p denotes pressure, and the subscripts denote the variable that is held constant in the derivative. The resulting slope s_p is in units of hectopascals per kilometer and is converted to meters (vertical) per kilometer (horizontal) using the hypsometric equation assuming a scale height of 7 km and a reference pressure of 1000 hPa.

The isentropic slope affects wavelike variability not only through its relation to baroclinic instability, but also through its projection onto the meridional gradient of potential vorticity (PV) along isentropic surfaces. For example, the meridional gradient in PV along isentropic surfaces can be written as

$$\left(\frac{\partial P}{\partial y}\right)_\theta = \left(\frac{\partial P}{\partial y}\right)_p + s_p\frac{\partial P}{\partial p} \simeq P\left(\frac{\beta}{f} - \frac{\partial s_p}{\partial p}\right), \quad (1)$$

where P denotes the zonal-mean potential vorticity. Here we have neglected the relative vorticity contribution to zonal-mean PV—that is, we have made the "planetary approximation" so that $P \simeq -gf(\partial\theta/\partial p)$. As evidenced in (1), the vertical derivative of the isentropic slope is directly related to the meridional PV gradient and thus is a central component of the index of refraction for wave propagation.

Figure 3a explores the linkages between the zonal-mean eddy fluxes of heat at 700 hPa ($[v^*T^*]_{700\text{hPa}}$) and the zonal-mean isentropic slope at 285 K ($s_{285\text{K}}$; the 285-K

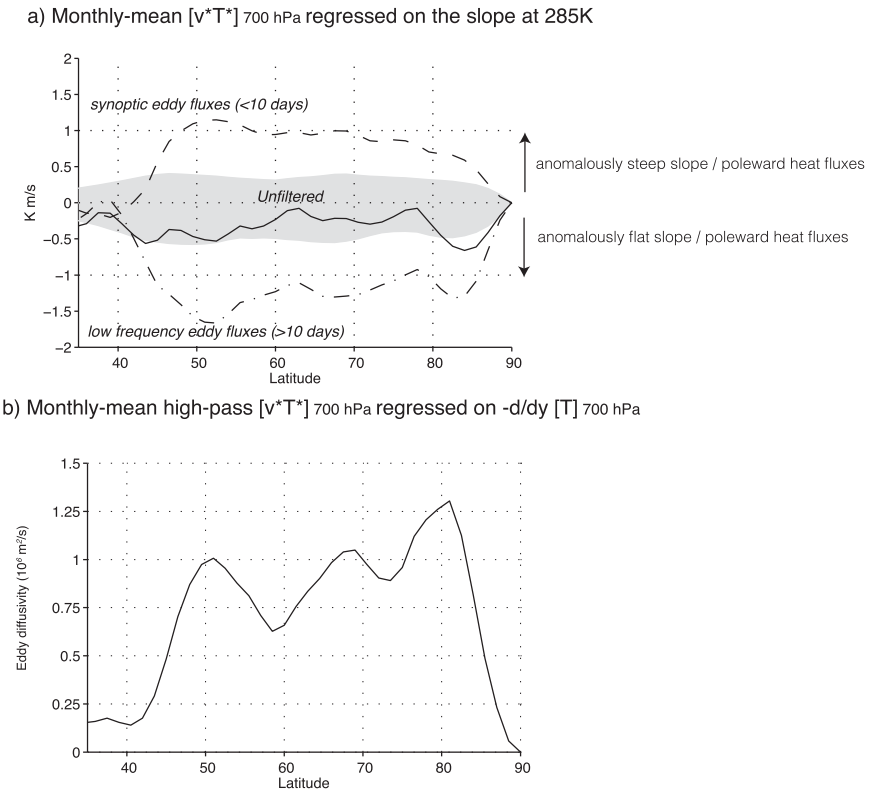

FIG. 3. (a) Regression of monthly mean values of the eddy heat flux at 700 hPa onto standardized values of the isentropic slope at 285 K. The solid line denotes results for unfiltered data, the dashed line is for the eddy fluxes of heat calculated from wind and temperature data that have been 10-day high-pass filtered (i.e., the synoptic eddy fluxes), and the dash-dotted line is for data that have been 10-day low-pass filtered (i.e., the low-frequency eddy fluxes). Units are K m s^{-1} per standard deviation fluctuation in the slope. (b) Regression of monthly mean values of the synoptic eddy heat fluxes at 700 hPa onto standardized values of the meridional temperature gradient at 700 hPa. The results are multiplied by −1 and are equivalent to the eddy diffusivity on monthly time scales (see text for details). All regressions are calculated as a function of latitude (e.g., the coefficients at 55°N denote the regression of the heat flux at 55°N onto the slope or temperature gradient at 55°N). Results are based on anomalies for the NH winter months (DJF). Shading in (a) above (below) the zero line denotes the 95% significance bounds for the synoptic (low frequency) eddy fluxes based on 1 degree of freedom per winter month (significant results exceed the shaded regions).

isentrope spans the lower troposphere at mid- to high latitudes; see Fig. 2). The results are calculated for monthly mean anomaly data and for the winter season months of DJF. The solid line shows unfiltered values of $[v^*T^*]_{700\text{hPa}}$ regressed onto standardized values of $s_{285\text{K}}$ as a function of latitude (e.g., the coefficient at 55°N corresponds to the regression of $[v^*T^*]_{700\text{hPa}}$ at 55°N onto standardized values of $s_{285\text{K}}$ at 55°N). The dashed and dot-dashed lines show corresponding results calculated for the synoptic and low-frequency eddy heat fluxes, respectively. Results are not shown for latitude bands where the 285-K surface intersects the earth's surface (equatorward of about 35°N).

The unfiltered eddy heat fluxes are negatively correlated with the isentropic slope at all latitudes, but the regression coefficients are weak and are not statistically significant (the 95% significance bounds are given by the light shading and are described in the figure caption). Interestingly, the synoptic (dashed) and low-frequency (dot-dashed) eddy heat fluxes exhibit highly significant but opposite-signed relationships with the slope. Anomalously steep isentropic slopes are associated with 1) anomalously poleward heat fluxes by synoptic eddies but 2) anomalously equatorward heat fluxes by low-frequency eddies. That is, the anomalous synoptic eddy heat fluxes are anomalously downgradient (down the anomalous meridional temperature gradient) whereas the anomalous low-frequency eddy heat fluxes are countergradient (up the anomalous meridional temperature gradient).

The eddy fluxes of heat at 700 hPa are a proxy for the eddy fluxes of PV and thus the generation of wave

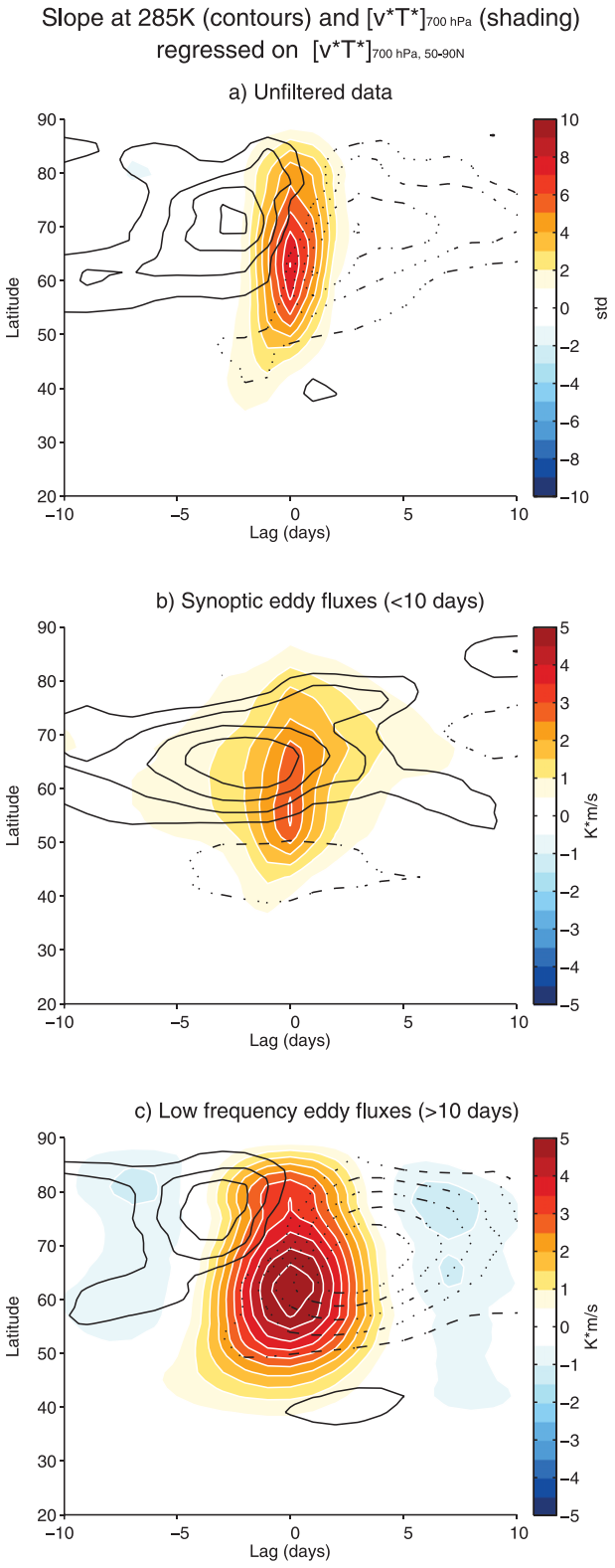

FIG. 4. Lag regressions based on standardized values of the eddy fluxes of heat at 700 hPa averaged over 50°–90°N. Results are shown as a function of lag and latitude. Shading denotes the eddy fluxes of heat at 700 hPa (K m s^{-1}). Contours denote the isentropic slope at 285 K [contours at 20 m (vertical) (1000 km)$^{-1}$ (meridional)]. Results are calculated for (a) the unfiltered heat fluxes, (b) the synoptic eddy heat fluxes, and (c) the low-frequency eddy heat fluxes. All results are based on zonal-mean, daily mean anomaly data (i.e., the seasonal cycle has been removed from the data) for DJF. The zero contour is omitted in all panels.

activity at the lower boundary (i.e., the divergence of the eddy heat flux at the surface; Held and Schneider 1999). Thus, the in-phase relationship between anomalies in the slope and the synoptic eddy heat flux is consistent with theories of baroclinic instability (i.e., anomalously steep isentropes lead to increased baroclinic wave generation and thus anomalously poleward eddy heat fluxes, and vice versa). The diffusive nature of baroclinic eddies has been clearly established in the context of the long-term-mean climatology (e.g., Kushner and Held 1998) but to our knowledge has not been quantified in the context of month-to-month variability in the isentropic slope. The out-of-phase relationship between anomalies in the slope and the low-frequency eddy heat flux is consistent with forcing of zonal-mean temperature by the eddy heat flux convergence (i.e., anomalously poleward eddy heat fluxes act to flatten the isentropic slope, and vice versa).

The month-to-month "synoptic eddy diffusivity" can be estimated by regressing the (anomalous) zonal mean synoptic eddy heat flux at 700 hPa $[v^*T^*]^{\text{synoptic}}_{700\text{hPa}}$ onto the (anomalous) meridional temperature gradient at 700 hPa $(\partial/\partial y)T_{700\text{hPa}}$. That is,

$$[v^*T^*]^{\text{synoptic}}_{700\text{hPa}} = -D\frac{\partial}{\partial y}T_{700\text{hPa}},$$

where the regression coefficient D provides an estimate of the synoptic eddy diffusivity on month-to-month time scales. The resulting values of D (Fig. 3b) suggest that the diffusivity of the synoptic eddies on month-to-month time scales is roughly $+1 \times 10^6$ m^2 s^{-1}; that is, the poleward eddy fluxes of heat are decreased by roughly 1 K m s^{-1} for every 1 K (1000 km)$^{-1}$ decrease in the amplitude of the equator–pole temperature gradient. The diffusivity estimates in Fig. 3b are the same order of magnitude (but half as large) as those calculated in Kushner and Held (1998), where the diffusivity is estimated from the climatological mean variance of the eddy streamfunction [see the full rhs of their (2)].

Figure 4 examines the linkages between the slope and eddy heat fluxes as a function of lag in daily data. In this case, the isentropic slope at 285 K and the eddy heat fluxes at 700 hPa are regressed as a function of lag and latitude onto a time series of the eddy heat fluxes averaged over 50°–90°N (hereafter denoted $[v^*T^*]_{50\text{–}90\text{N},700\text{hPa}}$). Lags

less than zero denote results that precede peak amplitude in $[v^*T^*]_{50\text{–}90N,700hPa}$, and vice versa. Figure 4a shows results for unfiltered eddies, Fig. 4b for synoptic eddies, and Fig. 4c for low-frequency eddies. Note that the shading range in Fig. 4a is different from that used in Figs. 4b,c.

By construction, in all panels the anomalous heat fluxes (shading) peak at lag 0 and at middle to high latitudes. The synoptic eddy heat fluxes are generally positive at all lags (Fig. 4b); the low-frequency eddy heat fluxes exhibit more pronounced quasi-periodic behavior with a time scale of about 2 weeks (Fig. 4c; note the negative regression coefficients at lags of about −7 and +7 days). The amplitudes of the low-frequency eddy heat fluxes are roughly twice those of the synoptic eddy heat fluxes.

The unfiltered heat fluxes are associated with opposite-signed isentropic slope anomalies during the periods before and after peak amplitude in mid- to high-latitude wave generation (Fig. 4a). The approximately 5–10-day period before peak wave generation is marked by increases in the isentropic slope poleward of 50°N; the period following peak wave generation is marked by decreases in the isentropic slope over middle and high latitudes. Hence, as summarized schematically in Figures 1a and 1b, periods of anomalous tropospheric wave generation are 1) preceded by anomalously steep isentropic slopes consistent with anomalous instability of the mean flow and 2) followed by anomalously flat isentropic surfaces consistent with the stabilizing effect of the resulting residual circulation (Fig. 1b). Note that the net change in the isentropic slope is very small when integrated over lags −10 to +10, as expected from the weak monthly mean regression coefficients given by the solid line in Fig. 3a.

The synoptic eddy heat fluxes are dominated by positive correlations with the isentropic slope that peak several days before lag 0 (Fig. 4b). Lag correlations do not prove causality. Nevertheless, the peak in the lag correlations before lag 0 is consistent with forcing of the synoptic eddy heat fluxes by variability in the isentropic slope (i.e., anomalously steep slopes lead to anomalous wave generation). In contrast, the rapid damping of the slope anomalies after lag 0 is consistent with forcing of the slope by the anomalous wave breaking aloft (see also Fig. 1b).

The low-frequency eddy heat fluxes are dominated by large negative correlations with the isentropic slope at positive lag (Fig. 4c). Again, the negative tendency in the slope after lag 0 is consistent with forcing of the slope by the anomalous wave breaking aloft. The comparatively weak positive correlations at negative lag are limited to very high latitudes. The apparent precursor in the slope in Fig. 4c may reflect the sensitivity of low-frequency eddies to the configuration of the flow, but it is also due at least in part to the periodicity inherent in the low-frequency eddy forcing (i.e., the positive slope anomalies between days −5 and 0 follow a period of negative heat fluxes anomalies between days −5 and −10).

The changes in the isentropic slope evident in Fig. 4 are due primarily to fluctuations in temperatures and therefore to the height of the isentropic surfaces at polar latitudes. The top row in Fig. 5 shows zonal-mean pressure on isentropic surfaces regressed onto standardized values of the $[v^*T^*]_{50\text{–}90N,700hPa}$ index time series as a function of isentropic level and latitude, averaged over lags (left) −10 to 0 days and (right) 0 to +10 days. The middle and bottom rows show results for the synoptic and low-frequency eddy heat fluxes, respectively. The 10-day period before peak heat fluxes is marked by anomalously low pressure on isentropic surfaces at polar latitudes (Fig. 5, top left), while the 10-day period after peak heat fluxes is marked by polar pressure anomalies in the opposite sense (Fig. 5, top right). As anticipated from Fig. 4, the precursor in the polar pressure field is most pronounced for the synoptic eddy fluxes (Fig. 5, middle left), whereas the response in the polar pressure field is most apparent for the low-frequency eddy fluxes (Fig. 5, bottom right).

Figure 6 is similar to Fig. 4 but shows zonal-mean temperature at 700 hPa (rather than the isentropic slope at 285 K) regressed onto the $[v^*T^*]_{50\text{–}90N,700hPa}$ time series for the unfiltered (Fig. 6a), synoptic (Fig. 6b), and low-frequency (Fig. 6c) eddy heat fluxes. Periods of anomalously poleward synoptic eddy heat fluxes are preceded by anomalously cool conditions over the polar cap (and, to a lesser extent, warm conditions near 50°N) that are consistent with the forcing of synoptic wave generation by anomalies in the meridional temperature gradient (Fig. 6b). Periods of anomalously poleward low-frequency eddy heat fluxes are 1) followed by anomalously warm conditions over the polar cap that are consistent with increased wave-driving aloft and 2) preceded by comparatively weak cool conditions that are at least partially due to the anomalously equatorward heat fluxes between lags of −10 and −5 days (Fig. 6c).

To what extent do the changes in the eddy fluxes of heat project onto variability in the momentum fluxes at the tropopause level (i.e., as expected from the life cycle of vertically and meridionally propagating tropospheric waves)? Figure 7 is identical to Fig. 6, but the contours now show the eddy momentum flux at 300 hPa regressed onto the $[v^*T^*]_{50\text{–}90N,700hPa}$ time series for the unfiltered (Fig. 7a), synoptic (Fig. 7b), and low-frequency (Fig. 7c) wave fluxes. The results in Fig. 7 are consistent with the life cycle of tropospheric waves (e.g., Simmons

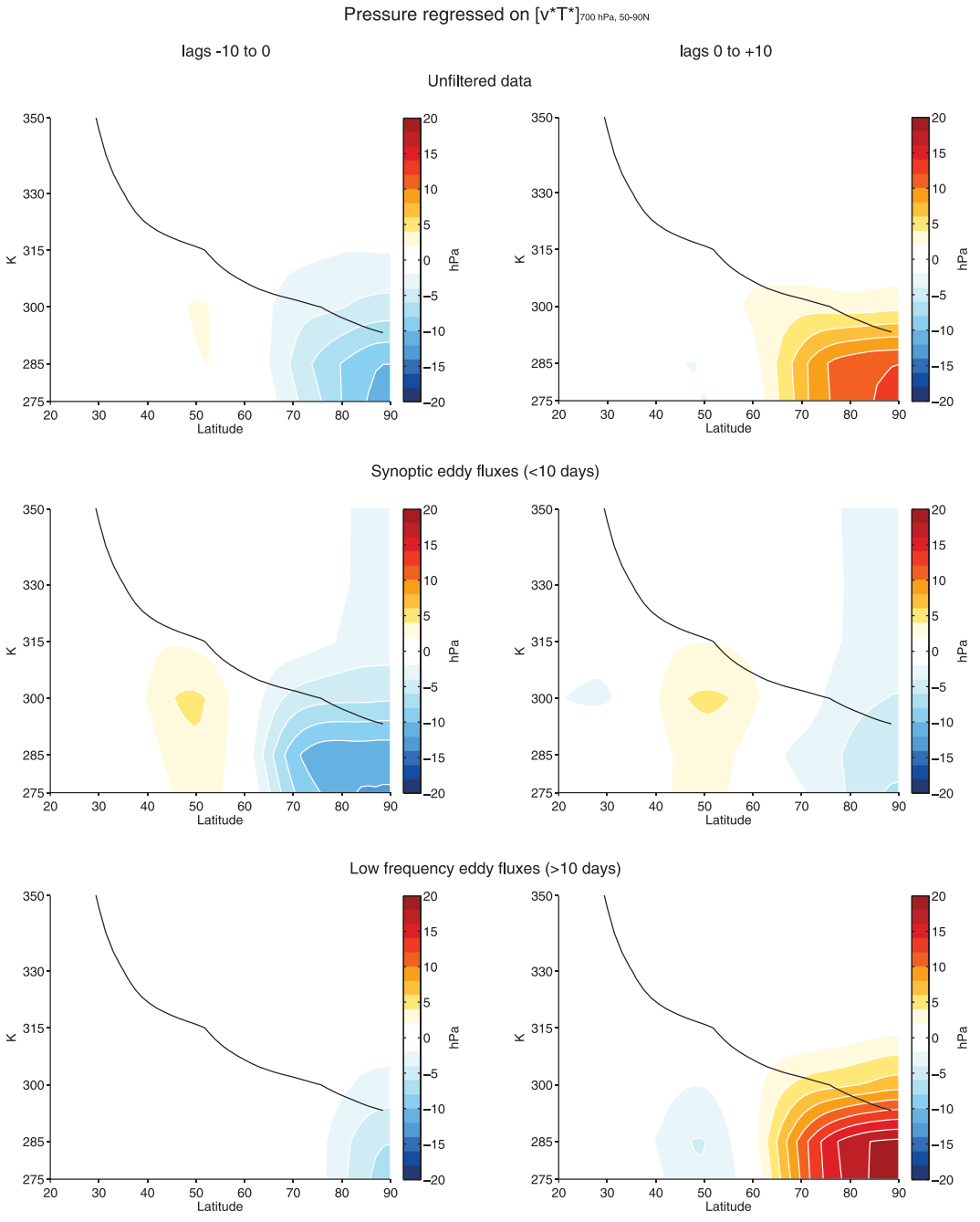

FIG. 5. Regressions on standardized values of the eddy fluxes of heat at 700 hPa averaged over 50°–90°N, for pressure anomalies averaged over (left) lags −10 to 0 (preceding the heat flux index) and (right) lags 0 to +10 (following the heat flux index). Results are calculated for (top) the unfiltered heat fluxes, (middle) the synoptic eddy heat fluxes, and (bottom) the low-frequency eddy heat fluxes. Pressure results are based on zonal-mean, daily mean anomaly data for DJF. The solid line indicates the 2-PVU isoline and thus approximates the height of the dynamical tropopause.

and Hoskins 1978; Edmon et al. 1980): periods of enhanced wave generation in the mid- to high-latitude lower troposphere are followed by anomalously equatorward wave activity fluxes (and thus anomalously poleward momentum fluxes) at the tropopause level. The same relationship holds true for both the synoptic (Fig. 7b) and low-frequency (Fig. 7c) eddies. The associated correlations peak around $r \sim 0.35$ (not shown),

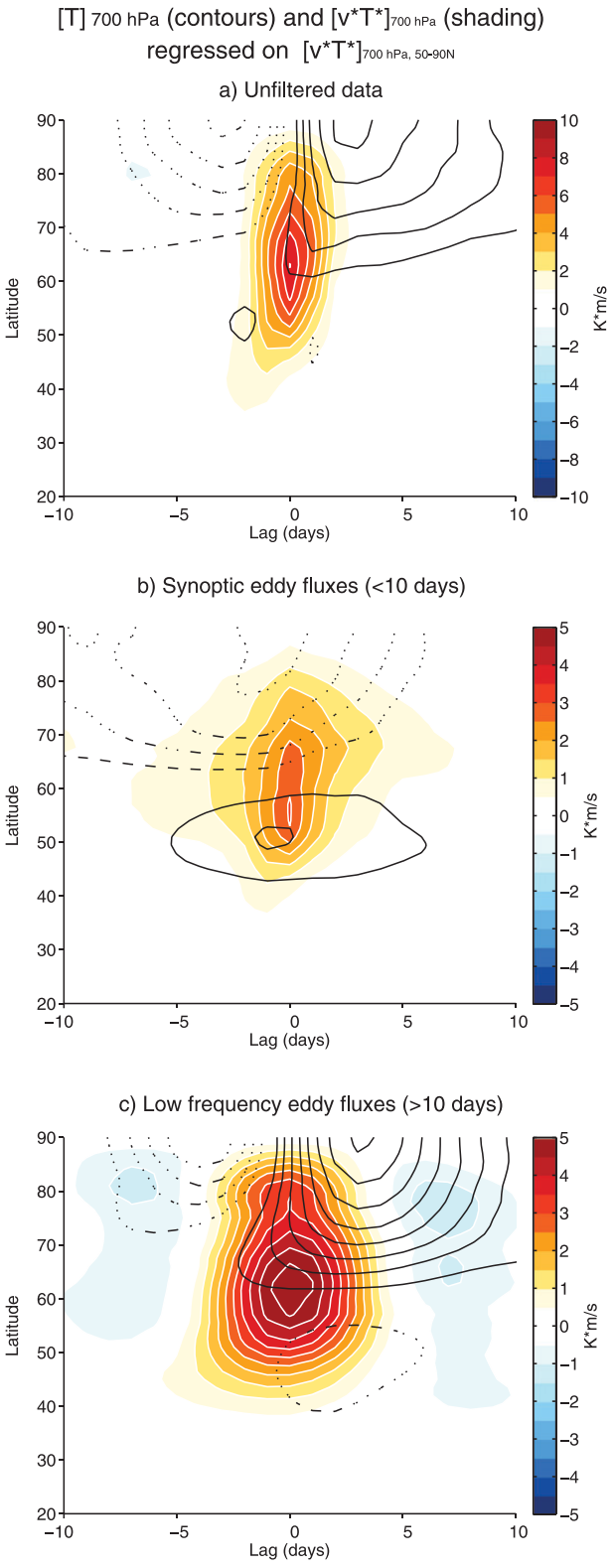

FIG. 6. As in Fig. 4, but contours denote temperatures at 700 hPa (contours at 0.2 K).

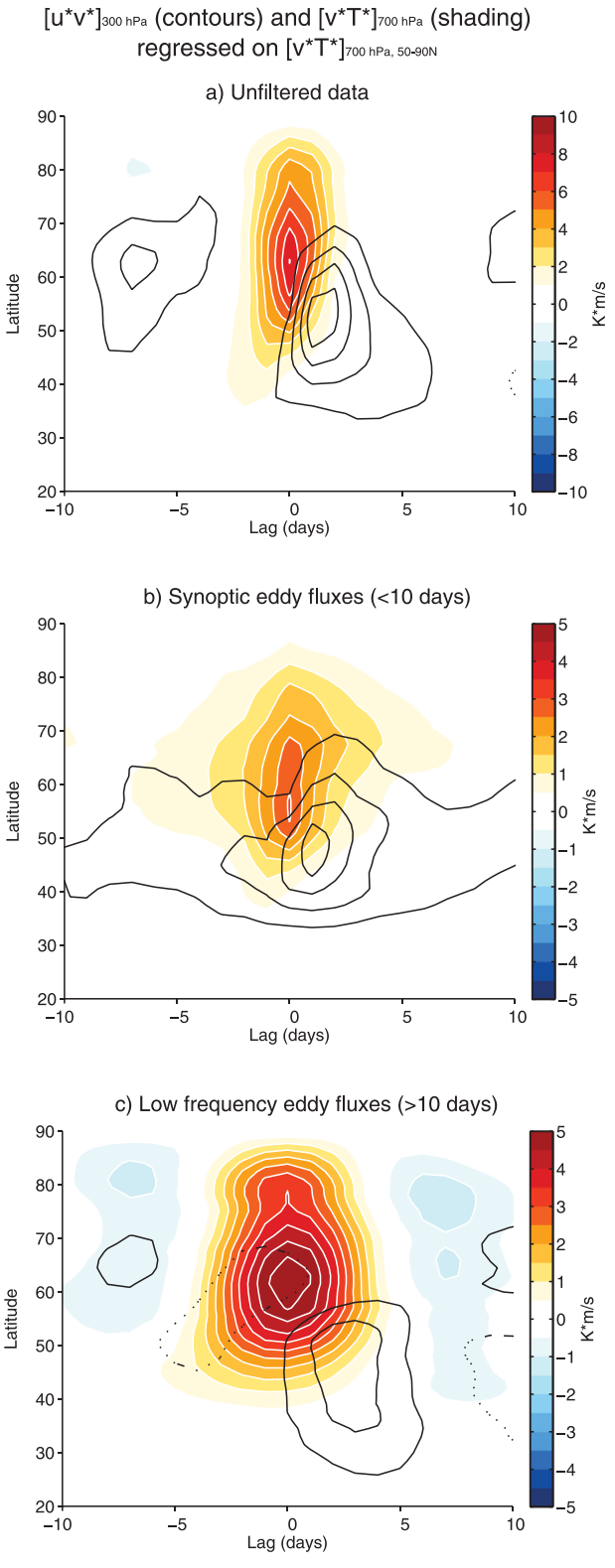

FIG. 7. As in Fig. 4, but contours denote the eddy fluxes of momentum at 300 hPa (contours at 2.25 $m^2 s^{-2}$).

and thus variations in the generation of wave activity over mid to high latitudes account for at most approximately 10% of the day-to-day variance in the momentum fluxes at middle latitudes. The remaining fraction is likely due to either 1) internal variability in the momentum fluxes that is independent of variability in the heat fluxes and/or 2) anomalous wave generation that is not captured by the heat flux index used to generate the figure.

The most important result in this section is the apparent causal linkage between variability in the isentropic slope and the generation of baroclinic waves. Such a linkage is widely accepted in the context of the climatological-mean circulation (i.e., baroclinic waves develop primarily in regions of large baroclinicity). But to our knowledge, such a linkage has not been clearly demonstrated in the context of day-to-day and month-to-month variability in the isentropic slope. Both the sign and lead/lag nature of the results suggest a causal relationship between the slope and the synoptic eddy heat fluxes: the synoptic eddy fluxes of heat are anomalously downgradient and thus cannot drive the attendant changes in the temperature field (Figs. 3a, 4b, and 6b); the largest synoptic eddy flux anomalies lag variability in the isentropic slope by several days (Fig. 4b). The linkages are highly significant (Fig. 3a) and the precursor in the temperature field (Fig. 6a) cannot be explained as an artifact of the (quasi-random) periodicity inherent in the eddy forcing. In the following section we will discuss the implications of the central results for large-scale climate variability.

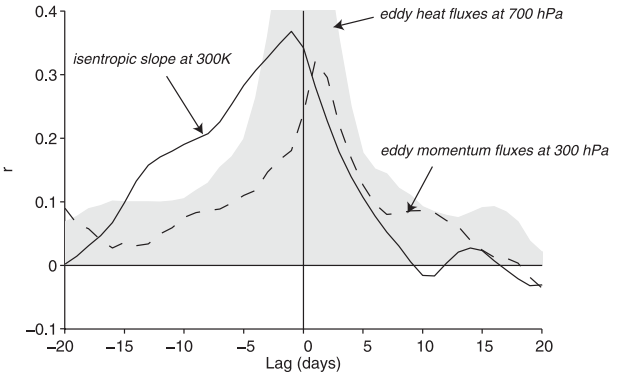

FIG. 8. Shading indicates the autocorrelation of the synoptic eddy fluxes of heat at 700 hPa averaged over 50°–90°N. Solid lines indicate lag correlations between the isentropic slope at 285 K averaged over 50°–90°N and the synoptic eddy fluxes of heat at 700 hPa averaged over 50°–90°N. Dashed lines indicate lag correlations between the eddy fluxes of momentum at 300 hPa averaged over 20°–70°N and the synoptic time scale eddy fluxes of heat at 700 hPa averaged over 50°–90°N. Negative lags denote the slope or momentum fluxes leading. Values exceeding $r = 0.09$ are significant at the 95% level based on a one-tailed test of the t statistic (the effective degrees of freedom are estimated based on the observed autocorrelation characteristics of the heat flux and slope time series).

4. Discussion

The influence of the mean flow on the eddy fluxes of heat and momentum can be viewed via two processes: 1) via wave propagation and dissipation in the free troposphere and 2) via the generation of wave activity near the earth's surface. Both are clearly important in the earth's atmosphere. The configuration of the mean flow determines the ''index of refraction'' for wave propagation and the regions for wave breaking. The tropospheric isentropic slope affects the generation of wave activity in the lower troposphere as well as the characteristics of wave propagation. Here we have focused on the relationship between the slope of the isentropic surfaces and the generation of wave activity in the lower troposphere.

The isentropic slope is related to the potential energy available to generate atmospheric eddies (e.g., Lorenz 1955; O'Gorman 2010), is of fundamental importance for baroclinic wave generation (e.g., Stone 1978; Stone and Nemet 1996), is intimately related to the growth rate in theories of baroclinic instability (e.g., Lindzen and Farrell 1980), and is directly related to the meridional PV gradient and thus the index of refraction for wave propagation (section 3). The results in section 3 reveal three aspects of the linkages between the isentropic slope and the wave fluxes of heat and momentum: 1) periods of increased isentropic slope are linked to enhanced generation of synoptic eddies near the surface; 2) enhanced generation of wave activity near the surface is linked to a rapid flattening of the isentropic slope that is consistent with increased wave dissipation aloft; and 3) enhanced generation of wave activity near the surface is followed by several days by anomalous eddy momentum fluxes aloft that are consistent with the life cycle of vertically and horizontally propagating waves. The results suggest that about 10% of the variance in the upper-tropospheric wave fluxes of momentum is linked directly to variability in the source of wave activity in the mid- to high-latitude lower troposphere.

Of the results shown in section 3, by far the most noteworthy are the observed relationships between variability in the isentropic slope and the generation of synoptic eddies. As summarized in Fig. 8, periods of anomalously large synoptic eddy heat fluxes over the middle to high latitudes (shading) are preceded by periods of anomalously steep isentropic surfaces (solid line) and followed by anomalously large momentum fluxes at 300 hPa (dashed line). The apparent causal linkage between the slope and the synoptic eddy heat

fluxes is consistent with the dynamics of developing baroclinic waves (Stone 1978; Stone and Nemet 1996), the close relationship between available potential energy and the amplitude of the wave component of the flow (e.g., O'Gorman 2010), and the ''macroturbulent'' view of atmospheric eddies (e.g., Held 1999). As noted above such a linkage has been demonstrated in the context of the long-term mean circulation (e.g., Kushner and Held 1998) and is presumed to underlie the dynamics of the annular modes (e.g., Robinson 1991, 2000), but has not been demonstrated conclusively in the context of day-to-day and month-to-month variability in the isentropic slope. We were unable to find similarly robust evidence of a direct causal linkage between variations in the mean flow and the eddy fluxes of momentum.

The observed relationships between variations in the isentropic slope and the generation of synoptic eddies have potentially important implications for understanding the extratropical circulation response to a range of forcings. The following are some examples:

1) The annular modes are theorized to derive in part from feedbacks between the momentum fluxes aloft, lower-tropospheric baroclinicity, and the generation of baroclinic waves (e.g., Robinson 2000; Lorenz and Hartmann 2001, 2003). The annular mode dynamics envisioned in Robinson (1991) and the corresponding feedback loop articulated in Robinson (2000) hinge on the forcing of anomalous wave activity by changes in the lower-tropospheric isentropic slope. The results in section 3 provide observational support for such forcing.
2) A range of forcings are predicted to drive changes in the storm tracks via their influence on the baroclinicity and thus isentropic slope in the extratropics. Increasing greenhouse gases are predicted to steepen the extratropical isentropic slope via changes in both the horizontal temperature gradient and static stability (e.g., Kushner et al. 2001; Yin 2005; Frierson 2006; Lu et al. 2008, 2010; Chen et al. 2010; O'Gorman 2010; Scaife et al. 2012; Butler et al. 2011); Antarctic ozone depletion is predicted to steepen the isentropic slope at southern high latitudes through the radiative effects of the Antarctic ozone hole (Grise et al. 2009); and midlatitude sea surface temperatures anomalies are predicted to perturb surface baroclinicity in the vicinity of the extratropical storm tracks (e.g., Kushnir et al. 2002, and references therein; Brayshaw et al. 2008). The results in section 3 provide observational support for a robust response in tropospheric wave generation to such changes in the isentropic slope.
3) Finally, wave-driven changes in the stratospheric circulation (e.g., sudden stratospheric warmings) are expected to drive variability in the tropospheric isentropic slope due to the downward penetrating mass circulation (e.g., Haynes et al. 1991; Song and Robinson 2004; Thompson et al. 2006). The relationships between stratospheric variability and the tropospheric isentropic slope are considered in Fig. 9.

Figure 9 shows latitude/potential temperature cross sections of the zonal-mean zonal wind (Fig. 9a); the zonal-mean pressure field (Fig. 9b); and the isentropic slope (Fig. 9c) regressed onto inverted values of the NAM10 index averaged over lags −10 days to +10 days (see section 2 for details of the index). Anomalously high pressure on an isentropic surface is equivalent to anomalously high potential temperature on nearby pressure surfaces. Thus, the results in Fig. 9b indicate the anomalies in the diabatic (residual mass) circulation associated with weakenings of the stratospheric vortex. Similar results are derived for regressions based on monthly mean data (not shown).

The results in Fig. 9a have been shown in numerous previous studies (e.g., Thompson and Wallace 2000; Baldwin and Dunkerton 2001; Limpasuvan et al. 2004): weakenings of the stratospheric vortex are coupled with westward anomalies centered near 55° and eastward anomalies centered near 35° that extend to the surface of the earth. The regressions for pressure on isentropic surfaces (Fig. 9b) must be in geostrophic and hydrostatic balance with the wind anomalies in Fig. 9a, but they are interesting in that they make explicit the depth of the downward-penetrating anomalous residual circulation. Weakenings of the stratospheric vortex are accompanied by anomalously downward residual motion not only in the polar stratosphere but in the polar troposphere as well (Fig. 9b; the anomalous residual circulation is nearly constant with height down to about 285 K at 65 N). As inferred from the changes in polar pressure, the isentropic slopes are anomalously flat throughout much of the midlatitude troposphere (Fig. 9c).

Limpasuvan et al. (2004) demonstrated that sudden stratospheric warmings are associated with 1) anomalously equatorward heat fluxes in the lower troposphere and 2) anomalously equatorward momentum fluxes near the tropopause level. Do the anomalously flat tropospheric isentropic slopes observed in associated with stratospheric variability (Fig. 9c) drive the changes in the eddy fluxes of heat and momentum revealed in Limpasuvan et al. (2004)? We have examined the linkages between the NAM10 index and the tropospheric wave fluxes of heat and momentum, and the results are mixed. The flattening of the mid- to high-latitude isentropic slopes revealed in Fig. 9c is accompanied by anomalously equatorward eddy fluxes of heat and

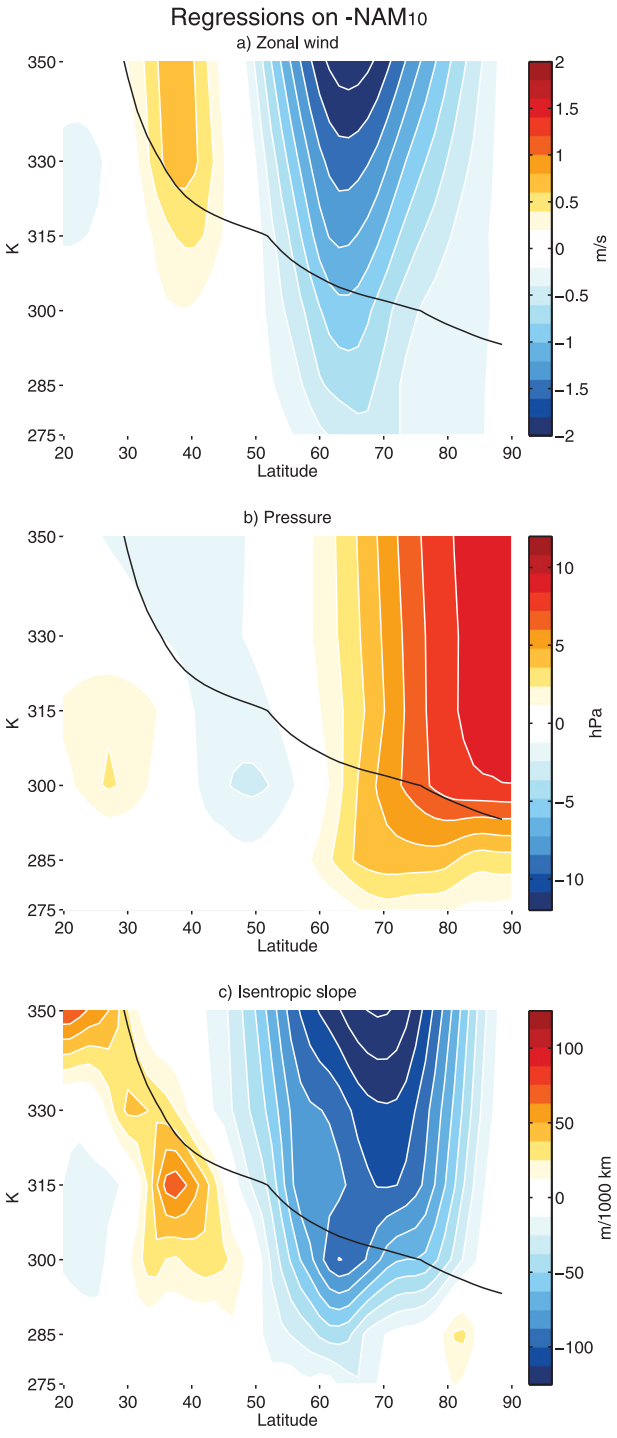

FIG. 9. Regressions based on inverted and standardized values of the NAM index at 10 hPa: (top) the zonal-mean zonal wind, (middle) the pressure on isentropic surfaces, and (bottom) the isentropic slope. Results are based on zonal-mean, daily mean anomaly data for DJF. Results are averaged over lags −10 days (preceding the NAM10 index) to +10 days (following the NAM10 index). The solid line indicates the 2-PVU isoline and thus approximates the height of the dynamical tropopause.

momentum at mid- to high latitudes (not shown). But the largest tropospheric eddy heat flux anomalies are due primarily to low-frequency eddies (rather than synoptic eddies, as inferred from Figs. 3 and 4). And the largest tropospheric eddy momentum flux anomalies precede the largest changes in the eddy heat fluxes (rather than follow, as inferred from Fig. 7). The linkages between stratospheric variability and the tropospheric mass circulation, isentropic slope, and wave fluxes of heat and momentum will be examined in detail in a future study.

Acknowledgments. We thank Walter Robinson and an anonymous reviewer for their insightful and helpful reviews. David W. J. Thompson and Thomas Birner are supported by the NSF Climate Dynamics Program.

REFERENCES

Baldwin, M. P., and T. J. Dunkerton, 2001: Stratospheric harbingers of anomalous weather regimes. *Science,* **294,** 581–584.

——, and D. W. J. Thompson, 2009: A critical comparison of stratosphere–troposphere coupling indices. *Quart. J. Roy. Meteor. Soc.,* **135,** 1661–1672.

Brayshaw, D. J., B. Hoskins, and M. Blackburn, 2008: The storm-track response to idealized SST perturbations in an aqua-planet GCM. *J. Atmos. Sci.,* **65,** 2842–2860.

Butler, A. H., D. W. J. Thompson, and T. Birner, 2011: Isentropic slopes, down-gradient eddy fluxes, and the extratropical atmospheric circulation response to tropical tropospheric heating. *J. Atmos. Sci.,* **68,** 2292–2305.

Chen, G., R. A. Plumb, and J. Lu, 2010: Sensitivities of zonal mean atmospheric circulation to SST warming in an aqua-planet model. *Geophys. Res. Lett.,* **37,** L12701, doi:10.1029/2010GL043473.

Dee, D. P., and Coauthors, 2011: The ERA-Interim reanalysis: Configuration and performance of the data assimilation system. *Quart. J. Roy. Meteor. Soc.,* **137,** 553–597, doi:10.1002/qj.828.

Edmon, H. J., Jr., B. J. Hoskins, and M. E. Mclntyre, 1980: Eliassen–Palm cross sections for the troposphere. *J. Atmos. Sci.,* **37,** 2600–2615.

Frierson, D. M. W., 2006: Robust increases in midlatitude static stability in simulations of global warming. *Geophys. Res. Lett.,* **33,** L24816, doi:10.1029/2006GL027504.

Grise, K. M., D. W. J. Thompson, and P. M. Forster, 2009: On the role of radiative processes in stratosphere–troposphere coupling. *J. Climate,* **22,** 4154–4161.

Haynes, P. H., M. E. Mclntyre, T. G. Shepherd, C. J. Marks, and K. P. Shine, 1991: On the "downward control" of extratropical diabatic circulations by eddy-induced mean zonal forces. *J. Atmos. Sci.,* **48,** 651–680.

Held, I. M., 1999: The macroturbulence of the troposphere. *Tellus,* **51,** 59–70.

——, and T. Schneider, 1999: The surface branch of the zonally averaged mass transport circulation in the troposphere. *J. Atmos. Sci.,* **56,** 1688–1697.

Holton, J. R., 2004: *An Introduction to Dynamic Meteorology.* 4th ed. Academic Press, 535 pp.

Kushner, P. J., and I. M. Held, 1998: A direct test, using atmospheric data, of a method for estimating oceanic diffusivity. *Geophys. Res. Lett.,* **25,** 4213–4216.

——, ——, and T. L. Delworth, 2001: Southern Hemisphere atmospheric circulation response to global warming. *J. Climate,* **14,** 2238–2249.

Kushnir, Y., W. A. Robinson, I. Bladé, N. M. J. Hall, S. Peng, and R. Sutton, 2002: Atmospheric GCM response to extratropical SST anomalies: synthesis and evaluation. *J. Climate,* **15,** 2233–2256.

Lau, N.-C., H. Tennekes, and J. M. Wallace, 1978: Maintenance of the momentum flux by transient eddies in the upper troposphere. *J. Atmos. Sci.,* **35,** 139–147.

Lim, G. H., and J. M. Wallace, 1991: Structure and evolution of baroclinic waves as inferred from regression analysis. *J. Atmos. Sci.,* **48,** 1718–1732.

Limpasuvan, V., D. W. J. Thompson, and D. L. Hartmann, 2004: The life cycle of the Northern Hemisphere sudden stratospheric warmings. *J. Climate,* **17,** 2584–2596.

Lindzen, R. S., and B. F. Farrell, 1980: A simple approximate result for the maximum growth rate of baroclinic instabilities. *J. Atmos. Sci.,* **37,** 1648–1654.

Lorenz, D. J., and D. L. Hartmann, 2001: Eddy–zonal flow feedback in the Southern Hemisphere. *J. Atmos. Sci.,* **58,** 3312–3327.

——, and ——, 2003: Eddy–zonal flow feedback in the Northern Hemisphere winter. *J. Climate,* **16,** 1212–1227.

Lorenz, E. N., 1955: Available potential energy and the maintenance of the general circulation. *Tellus,* **7,** 157–167.

Lu, J., G. Chen, and D. M. W. Frierson, 2008: Response of the zonal mean atmospheric circulation to El Nino versus global warming. *J. Climate,* **21,** 5835–5851.

——, ——, and ——, 2010: The position of the midlatitude storm track and eddy-driven westerlies in aquaplanet AGCMs. *J. Atmos. Sci.,* **67,** 3984–4000.

O'Gorman, P. A., 2010: Understanding the varied response of the extratropical storm tracks to climate change. *Proc. Natl. Acad. Sci. USA,* **107,** 19 176–19 180.

Robinson, W. A., 1991: The dynamics of the zonal index in a simple model of the atmosphere. *Tellus,* **43A,** 295–305.

——, 2000: A baroclinic mechanism for the eddy feedback on the zonal index. *J. Atmos. Sci.,* **57,** 415–422.

——, 2006: On the self-maintenance of midlatitude jets. *J. Atmos. Sci.,* **63,** 2109–2122.

Scaife, A. A., and Coauthors, 2012: Climate change projections and stratosphere–troposphere coupling. *Climate Dyn.,* **38,** 2089–2097, doi:10.1007/s00382-011-1080-7.

Simmons, A. J., and B. J. Hoskins, 1978: The life cycles of some nonlinear baroclinic waves. *J. Atmos. Sci.,* **35,** 414–432.

Song, Y., and W. A. Robinson, 2004: Dynamical mechanisms for stratospheric influences on the troposphere. *J. Atmos. Sci.,* **61,** 1711–1725.

Stone, P. H., 1978: Baroclinic adjustment. *J. Atmos. Sci.,* **35,** 561–571.

——, and B. Nemet, 1996: Baroclinic adjustment: A comparison between theory, observations, and models. *J. Atmos. Sci.,* **53,** 1663–1674.

Thompson, D. W. J., and J. M. Wallace, 2000: Annular modes in the extratropical circulation. Part I: Month-to-month variability. *J. Climate,* **13,** 1000–1016.

——, J. C. Furtado, and T. G. Shepherd, 2006: On the tropospheric response to anomalous stratospheric wave drag and radiative heating. *J. Atmos. Sci.,* **63,** 2616–2629.

Vallis, G. K., 2006. *Atmospheric and Oceanic Fluid Dynamics.* Cambridge University Press, 745 pp.

Yin, J. H., 2005: A consistent poleward shift of the storm tracks in simulations of 21st century climate. *Geophys. Res. Lett.,* **32,** L18701, doi:10.1029/2005GL023684.